Beam tracing description of non-Gaussian wave beams

Christos Tsironis*
Department of Physics, Aristotle University of Thessaloniki, 54124 Thessaloniki, Greece

Emanuele Poli† and Grigory V. Pereverzev‡
Max-Planck-Institut für Plasmaphysik, D-85748 Garching bei München, Germany

In experiments involving electron-cyclotron waves, beams with a non-Gaussian amplitude profile can be generated by the launching system or during the propagation in the plasma. The propagation and absorption of non-Gaussian beams is formulated in terms of the beam tracing asymptotic technique. The proper sequence for tracing arbitrary beams has been established, which involves the formulation of the decomposition of arbitrary electric field profiles into Gaussian-Hermite modes, the generalization of the beam width parameter and the damping of higher-order modes. The effect of the phase-shift of the modes (with respect to the beam axis) is analyzed within beam tracing and included in the description of the beam. As an application, we consider the propagation and absorption of multi-mode beams in a simplified plasma geometry, where a comparison with an exact solution is possible. Also, the properties of the propagation of a non-Gaussian beam in the transmission line of an EC launching system are analyzed.

PACS numbers: 41.20.Jb, 42.25.-p, 52.35.Hr, 52.50.Sw

I. INTRODUCTION

Electron Cyclotron Resonance Heating (ECRH) and Electron Cyclotron Current Drive (ECCD) are nowadays well-established methods for plasma heating and generation of non-inductive current in modern fusion devices (tokamaks, stellarators) [1–3], with their present usage going beyond their heating and current drive application. The control of MHD instabilities (e.g. sawtooth, NTM), the formation of ITBs, the tailoring of the current profile and the high resolution achieved in plasma diagnostics (interferometry, reflectometry) are examples of employing the advantage of the well-localized power deposition of EC waves (see e.g. [1] and references therein).

The propagation of EC waves in plasma is described by Maxwell's equations. In general, to obtain a full solution to the problem is very hard, because the wave equation is a PDE and also a constitutive relation for the plasma response must be provided. In situations where the wavelength is small compared to the scale length of inhomogeneity of the medium, which is mostly the case in modern experiments, a simplification is achieved by using asymptotic methods, i.e. ray tracing [4, 5], quasi-optics [6–8] or beam tracing [9, 10]. In ray/beam tracing, the solution is obtained through Hamiltonian ODEs where the dispersion function plays the role of the Hamiltonian. Such treatments provide a direct physical picture of the process in terms of Hamiltonian rays. In most applications, the cold plasma dispersion function [11] is used as the Hamiltonian function. This choice is justified by the fact that, apart from the very narrow region of resonant interaction, the wave-plasma interaction is very weak. The dielectric response of the plasma is mainly derived in terms of the linear theory of plasma oscillations [12, 13]. Such a simplified treatment is supported by the consideration that, for parameters relevant to modern experiments, the wave intensity is small and falls in the linear regime. There are several ray and beam tracing codes that implement the schemes described above (see e.g. Refs. 14–17) and the results obtained are in agreement with a number of transmission experiments from different tokamaks (details can be found in Refs. 1–3).

In the majority of ECRH and ECCD experiments, narrow beams with initial focusing are preferred: in heating experiments to increase the localization of EC absorption, in diagnostics to make the investigated region as small as possible and in instability control to achieve alignment with the "resonances" characterizing the instability. The state-of-the-art in theory and experiment is mainly based on Gaussian beams. They are employed in practical applications because of their low Ohmic losses in the transmission line and because they allow an easy coupling to waveguide modes. They are also easy to model in theoretical and numerical investigations.

However, the beam that enters the plasma might not always be Gaussian. This could be an undesired effect owed to a misalignment of the launching system or to a deformation of the steering mirror due to extreme heat load, or it could be intentionally set up. A typical example is the reduction of the power density on the window between the transmission line and the vacuum vessel, which can be achieved by adding up a higher-order mode [18] to the fundamental one in order to achieve a broader profile (see Sec. VI). Furthermore, in the plasma, a modification of the initial Gaussian beam shape might occur due to localized absorption, non-local redistribution of

*URL: http://www.astro.auth.gr/~ctsironis; Electronic address: ctsironis@astro.auth.gr
†URL: www.ipp.mpg.de/~emp; Electronic address: Emanuele.Poli@ipp.mpg.de
‡Electronic address: Grigory.Pereverzev@ipp.mpg.de

energy by resonant particles along the magnetic field line or vivid focusing and strong wave interference.

The, desirable or not, cases where non-Gaussian beams are coupled to the plasma, is a part that has not been significantly developed in the existing literature. In this paper, the beam tracing method [10] is applied to the propagation of arbitrary beams. After a brief review of the asymptotic methods for solving the wave equation, the sequence for tracing arbitrary beams is described and the changes required to the existing beam tracing theory are highlighted. Special attention is given to the description of the phase-shift of the modes (with respect to the beam axis) in terms of the beam tracing theory, as well as to the modelling of the absorption of higher-order modes. The simplified description through characteristic parameters (e.g. width, curvature radius) is retained by generalizing the parameters already defined for Gaussian beams. As applications, the propagation of non-Gaussian EC beams in simplified plasma geometry is studied, with a validation of the results, and also the advantageous properties of the transmission of non-Gaussian beams from an EC launcher to the plasma are illustrated.

II. ASYMPTOTIC METHODS FOR SOLVING THE WAVE EQUATION

The application of asymptotic methods to the solution of the wave equation, which for the (complex) harmonic field $\bar{\boldsymbol{E}}(\boldsymbol{r},t) = \bar{\boldsymbol{E}}(\boldsymbol{r})e^{-i\omega t}$ in an inhomogeneous medium with dielectric response $\hat{\varepsilon}$ reads

$$\nabla \times [\nabla \times \bar{\boldsymbol{E}}(\boldsymbol{r})] - \frac{\omega^2}{c^2}\hat{\varepsilon}(\boldsymbol{r},\omega)\cdot\bar{\boldsymbol{E}}(\boldsymbol{r}) = 0,$$

stems from Maxwell's equations. The approach amounts to describing the wave propagation in terms of a bundle of rays which are continuously refracted by a slowly space-varying medium, in the same way as the trajectory of a particle is deflected by a certain potential, a correspondence being established between the propagation of waves and the Hamiltonian theory for particles [19].

The pioneer method in this respect is the geometrical optics, or ray tracing, method [4, 5, 20, 21]. The wave field is described as a generalization of the standard form for the plane wave, known as the eikonal form

$$\bar{\boldsymbol{E}}(\boldsymbol{r}) = \bar{\boldsymbol{A}}(\boldsymbol{r})e^{i\kappa s(\boldsymbol{r})}, \tag{1}$$

where the function s (eikonal) is the generalization of the plane-wave phase $\boldsymbol{k}\cdot\boldsymbol{r}$ for weakly inhomogeneous medium and $\kappa = \omega L/c \gg 1$ the short-wavelength limit parameter, with L the typical inhomogeneity scale length. The connection of the eikonal and the wave-vector is the obvious $\boldsymbol{k} = \kappa\nabla s$. For each ray one can determine the "backbone" of the wave field by means of a set of ODEs that give the variation of the phase and the amplitude along the ray. These equations are obtained by exploiting an asymptotic series expansion of the solution sought in a neighborhood of the considered location and time

$$\bar{\boldsymbol{A}} = \bar{\boldsymbol{A}}_{\boldsymbol{0}} + \frac{\bar{\boldsymbol{A}}_{\boldsymbol{1}}}{\kappa} + \frac{\bar{A}_2}{\kappa^2} + ..., \tag{2}$$

inserting Eqs. (1), (2) in the wave equation and separating terms of different order in κ. The zero-order equation describes the phase behavior in space

$$\left[\kappa^2(-k^2\hat{\boldsymbol{I}} + \boldsymbol{kk}) + \hat{\varepsilon}^H\right]\cdot\bar{\boldsymbol{A}}_{\boldsymbol{0}} \equiv \hat{\boldsymbol{\Lambda}}\cdot\bar{\boldsymbol{A}}_{\boldsymbol{0}} = 0. \tag{3}$$

The solvability condition $\det[\hat{\Lambda}] \equiv H = 0$ is a Hamilton-Jacobi equation with respect to s. This results to the Hamiltonian ray equations, which trace the evolution of the wave trajectory and wave-number in the plasma

$$\frac{d\boldsymbol{r}}{d\tau} = \frac{\partial H}{\partial \boldsymbol{k}}, \quad \frac{d\boldsymbol{k}}{d\tau} = -\frac{\partial H}{\partial \boldsymbol{r}}. \tag{4}$$

The first-order equation gives the amplitude evolution along the ray

$$\frac{d|\bar{A}_0|^2}{d\tau} + (\nabla\cdot\boldsymbol{v}_g + 2\gamma)\,|\bar{A}_0|^2 = 0, \tag{5}$$

where $\gamma = \bar{\boldsymbol{e}}^*\cdot\hat{\varepsilon}^A\cdot\bar{\boldsymbol{e}}$ is the absorption coefficient and $\bar{\boldsymbol{e}}$ the polarization unit vector ($\bar{\boldsymbol{A}}_{\boldsymbol{0}} = \bar{A}_0\bar{\boldsymbol{e}}$). Eq. (5) implies that the wave energy propagates in the direction of the group velocity $\boldsymbol{v}_g \propto \partial H/\partial\boldsymbol{k}$, and the absorption is proportional to the projection of the anti-Hermitian part of the dielectric tensor $\hat{\varepsilon}^A$ onto the polarization vector.

The ray tracing approach provides an effective tool to solve Maxwell equations in the short-wavelength limit. However, there is the limitation that wave phenomena (e.g. diffraction) are not taken into account. In the formulation of geometrical optics, wave effects appear in the higher-order equations, which are, in general, difficult to treat. In situations where these effects cannot be neglected, for example when focused or collimated beams are used, the use of ray tracing leads to physical inconsistencies near foci or caustics. Methods that refine geometrical optics taking into account wave effects, referred to as quasi-optics methods, have been developed to deal with the variation of the beam width and the diffractive broadening of the beam cross-section. The complex geometrical optics [6, 8, 22, 23] takes the wave phase to be complex-valued, $\bar{s} = s + i\phi$, with the imaginary part being related to the transverse beam profile

$$\bar{\boldsymbol{E}}(\boldsymbol{r}) = \bar{\boldsymbol{A}}(\boldsymbol{r})e^{i\kappa\bar{s}(\boldsymbol{r})} = \bar{\boldsymbol{A}}(\boldsymbol{r})e^{i\kappa s(\boldsymbol{r})-\kappa\phi(\boldsymbol{r})}, \tag{6}$$

where the imaginary wave-vector $\mathrm{Im}(\bar{\boldsymbol{k}}) = \kappa\nabla\phi$ is normal to $\boldsymbol{v}_g$. Here, a new (intermediate) scale length comes into play, the beam width w ($\lambda \le w \le L$). Note that $\mathrm{Im}(\bar{\boldsymbol{k}}) \propto w^{-1}$ is of order $\kappa^{-1/2}$ with respect to $\mathrm{Re}(\bar{\boldsymbol{k}})$, as a result from the Fresnel condition $w^2 \ge \lambda L$. The corresponding complex solutions can be obtained by three different approaches. First, one can derive a set of Hamiltonian equations describing modified rays, based on a Taylor expansion in the complex dispersion relation, allowed

by $\mathrm{Im}(\bar{\boldsymbol{k}}) \ll Re(\bar{\boldsymbol{k}})$. The resulting dispersion function consists only of real terms, the zero-order term of geometrical optics and a higher-order term that describes the wave phenomena (see e.g. Refs. 6, 15). We can call this approach "quasi-optical ray tracing". On the other hand, one can extend the resulting equations in the complex space by means of an analytical continuation of the Hamiltonian, and then obtain a geometrical optics solution in the complex space. Thereafter, the physical wave field is obtained by evaluating the solution at a real-valued observation point (for details see Ref. 8).

The third approach is the beam tracing method. It combines the simplicity of ray tracing with a description of the wave properties. The electric field has the same form as in quasi-optics, however the amplitude expansion contains the intermediate order $\kappa^{-1/2}$ [9, 10]

$$\bar{\boldsymbol{A}} = \Phi_{mn}\bar{\boldsymbol{A}}_{\boldsymbol{0}} - \frac{\partial\Phi_{mn}}{\partial\xi_j}\frac{i\bar{\boldsymbol{A}}_{\boldsymbol{1}}^{j}}{\kappa^{1/2}} - \frac{\partial^2\Phi_{mn}}{\partial\xi_i\partial\xi_j}\frac{\bar{\boldsymbol{A}}_{\boldsymbol{2}}^{ij}}{2\kappa} - \Phi_{mn}\frac{i\bar{\boldsymbol{A}}_{\boldsymbol{3}}}{\kappa}. \quad (7)$$

The function Φ_{mn} describes the transverse beam profile

$$\Phi_{mn}(\xi_1,\xi_2) = \frac{H_m(\xi_1)H_n(\xi_2)}{\sqrt{\pi 2^{m+n}m!n!}}e^{-\phi(\xi_1,\xi_2)},$$

with H_n the Hermite polynomials. In the above, a system of dimensionless coordinates (τ,ξ_1,ξ_2) associated with the beam has been introduced, the "beam coordinates" (see Fig. 1), where τ is along and ξ_1,ξ_2 are across the propagation direction. The curve $\xi_1 = \xi_2 = 0$ is a geometrical-optics ray (called the reference ray) that describes the center of gravity of the beam and obeys the ray tracing equations as given in Eq. (4). ϕ is a quadratic form of ξ_1,ξ_2, and the transverse beam coordinates (ξ_1,ξ_2) are chosen such that the quadratic form 2ϕ is unitary, ie. $\phi = \delta_{ij}\xi_i\xi_j/2$. Around the reference ray, the complex phase of the wave field is expanded in Taylor series around the reference ray

$$\bar{s} = \bar{s}_0 + \bar{s}_\alpha(x_\alpha - x_{0\alpha}) + \frac{1}{2}\bar{s}_{\alpha\beta}(x_\alpha - x_{0\alpha})(x_\beta - x_{0\beta}), \quad (8)$$

this treatment being known as paraxial WKB (pWKB) expansion. The coefficients $\bar{s}_{\alpha\beta} = \partial^2\bar{s}/(\partial x_\alpha\partial x_\beta) = s_{\alpha\beta} + i\phi_{\alpha\beta}$ are determined by an ordinary differential equation emerging from the terms of order κ^{-1} in (7)

$$\frac{d\bar{s}_{\alpha\beta}}{d\tau} + \frac{\partial^2 H}{\partial x_\alpha\partial x_\beta} - \frac{\partial^2 H}{\partial x_\beta\partial k_\gamma}\bar{s}_{\alpha\gamma} - \frac{\partial^2 H}{\partial x_\alpha\partial k_\gamma}\bar{s}_{\beta\gamma} - \frac{\partial^2 H}{\partial k_\gamma\partial k_\delta}\bar{s}_{\alpha\gamma}\bar{s}_{\beta\delta} = 0. \quad (9)$$

The coefficients $s_{\alpha\beta}$ relate to the curvature radius ($\propto R^{-1}$), while $\phi_{\alpha\beta}$ relate to the beam width ($\propto W^{-2}$) and the connection with the lab coordinates is $2\phi = \delta_{ij}\xi_i\xi_j = \phi_{\alpha\beta}(x_\alpha - x_{0\alpha})(x_\beta - x_{0\beta})$. The amplitude transport equation is similar to Eq. (5)

$$\frac{d|\bar{C}_{mn}|^2}{d\tau} + \left[\nabla\cdot\boldsymbol{v}_g + 2\gamma(\boldsymbol{k})\right]|\bar{C}_{mn}|^2 = 0, \quad (10)$$

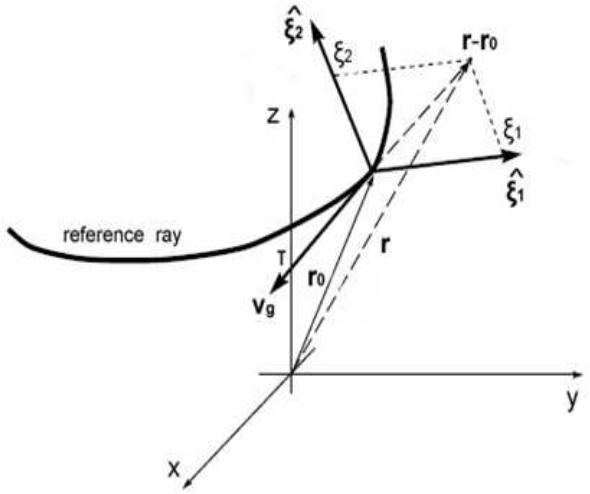

FIG. 1: The beam coordinate system (τ,ξ_1,ξ_2) (figure reprinted from Ref. 24).

however here absorption is calculated on the central ray but refers to the whole beam. $\bar{C}_{mn} = \bar{A}_0 e^{i\Theta_{mn}}$ is the geometrical-optics amplitude excluding the phase shift Θ_{mn} with respect to the reference ray (we will discuss later the exact definition of Θ_{mn}). Based on all the above, the general solution for the electric field can be expressed as a superposition of partial solutions, $\bar{\boldsymbol{E}} = \sum_{mn}\bar{E}_{mn}\bar{\boldsymbol{e}}$, of the form

$$\bar{E}_{mn} = \frac{\bar{C}_{mn}H_m(\xi_1)H_n(\xi_2)}{\sqrt{\pi 2^{m+n}m!n!}}e^{i\kappa s - \kappa\phi - i\Theta_{mn}}, \quad (11)$$

The partial solutions of (11) are a set of eigenmodes of the wave equation, known as Gaussian-Hermite modes (see further Sec. III).

The advantages of pWKB beam tracing over the other asymptotic methods are worthy of mention. First of all, it allows the inclusion of wave effects (neglected in standard ray tracing) using an even smaller number of equations. Moreover, this is achieved by means of ODEs in real space and therefore this method does not require one to solve a set of coupled ray equations (like in quasi-optical ray tracing) nor to integrate ray equations in complex space. The beam tracing equations are implemented in the code TORBEAM [16, 25], which calculates the propagation of Gaussian electron-cyclotron beams in a tokamak geometry, for arbitrary launching conditions and analytic or experimental magnetic equilibrium. Apart from the beam propagation, the spatial profiles of the power deposition and current drive are calculated based on linear models for the electron-cyclotron absorption and the current drive efficiency.

III. SEQUENCE FOR TRACING AN ARBITRARY BEAM

The propagation and absorption of Gaussian beams, i.e. beams with an initial Gaussian power profile, has been successfully followed in terms of all the asymptotic methods mentioned in Sec. II, both analytically and numerically (indicative Refs. 6, 10, 14–16, 24). In this part of the paper, we sketch the proper sequence in order to follow the propagation of a non-Gaussian beam in an inhomogeneous anisotropic plasma, in terms of the pWKB beam tracing method. We model the non-Gaussian beam as a superposition of Gaussian-Hermite modes, as given in Eq. (11). The modifications needed in the formulation presented in Ref. 10 in order to be able to study generic beams are also presented.

The beam tracing method is preferable because the specific formulation makes the inclusion of higher-order modes in a Gaussian beam more straightforward. The partial beam-tracing solutions $\{E_{mn}\}$ can be viewed as a complete set of eigenfunctions (modes) of the wave equation, as each one of the partial solutions satisfies the energy conservation, as expressed in (10), and in the weak absorption limit ($\epsilon^A \ll \epsilon^H$) there is no coupling between the different modes (m,n). Also, the mathematical expression for $|\bar{E}_{mn}|$ is linearly related to the Gaussian-Hermite functions $\varphi_n(x) = e^{-x^2/2}H_n(x)/\sqrt{\pi^{1/2}2^n n!}$

$$|\bar{E}_{mn}| = |\bar{C}_{mn}|\frac{H_m(\xi_1)H_n(\xi_2)}{\sqrt{\pi 2^{m+n}m!n!}}e^{-(\xi_1^2+\xi_2^2)/2} =$$
$$|\bar{C}_{mn}|\Phi_{mn}(\xi_1,\xi_2) = |\bar{C}_{mn}|\varphi_m(\xi_1)\varphi_n(\xi_2),$$

which are a complete and orthonormal basis in the space of both squared-integrable functions and rapidly decreasing smooth functions in two dimensions. Thus, an arbitrary electric field can be expressed as the superposition of such modes and, according to the previous section, analyzed with the beam tracing formalism. The specific sequence for the analysis is as follows: first, assign proper initial conditions to all the beam-tracing variables; second, solve for the reference ray, the wave-front curvature and the beam width, and also the amplitude transport equation for each beam mode (m,n).

Regarding the first step, the proper assignment of initial conditions for the variables involved in the beam tracing equations (4), (9) is by no means difficult, as these variables are calculated on the reference ray and thus are common for all the modes of the non-Gaussian beam. For the initial amplitudes of the modes $\bar{C}_{mn}|_{\tau=0}$, the fact that an arbitrary initial electric field distribution can be decomposed into a superposition of Gaussian-Hermite modes can be utilized. In fact, the coefficients of such an expansion of the initial field coincide with the initial values for the amplitudes in the beam tracing equations

$$\bar{E}(\xi_1,\xi_2)|_{\tau=0} = \sum_{mn}\bar{C}_{mn}|_{\tau=0}\phi_m(\xi_1)\phi_n(\xi_2). \quad (12)$$

The calculation of the expansion coefficients is based on the condition of orthogonality of the Gaussian-Hermite functions, as applied in Eq. (12)

$$\bar{C}_{mn}|_{\tau=0} = \int_{-\infty}^{\infty}\bar{E}(\xi_1,\xi_2)|_{\tau=0}\phi_m(\xi_1)\phi_n(\xi_2)d\xi_1 d\xi_2. \quad (13)$$

We should note that, in theory, in order to achieve the equality (12) an infinite number of modes is required. However, in practical applications, the number of modes is restricted to a finite number per transverse direction (M,N), and the role of the choice of (M,N) on the accuracy of the expansion should be investigated. The error in the expansion of the electric field may be defined as

$$Error = 1 - \frac{\sum_{m,n=0}^{M,N}\left|\bar{C}_{mn}|_{\tau=0}\right|^2}{\int_{-\infty}^{\infty}\left|\bar{E}(\xi_1,\xi_2)|_{\tau=0}\right|^2 d\xi_1 d\xi_2}, \quad (14)$$

a positive-definite quantity as implied by the Bessel inequality for generalized Fourier series.

As an example of the technique described here, we consider the decomposition of a real electric field with a one-dimensional square profile

$$E(\xi)|_{\tau=0} = E_0\left[h(\xi+d) - h(\xi-d)\right]. \quad (15)$$

In the previous relation, d is the width of the square profile, normalized to the same scale length W as the transverse coordinate ξ, and $h(x)$ is the Heaviside step function. By inserting (15) into the one-dimensional analog of (13), the coefficients for the expansion are found

$$C_n|_{\tau=0} = \frac{E_0}{\sqrt{\pi^{1/2}2^n n!}}\int_{-d}^{d}e^{-\xi^2/2}H_n(\xi)d\xi.$$

Notice here that, according to the properties of the Hermite polynomials, $C_n|_{\tau=0}$ is non-zero only for even values of the index n. We have given a numerical solution to the problem, and in Fig. 2(a) we show the amplitude profile of the square beam, reconstructed according to the results of the decomposition into Gaussian-Hermite modes using $N = 50$ modes. The approximation is in general very successful, and increasing the number of modes makes the approximation even better. In Fig. 2(b), the coefficients of the even modes are plotted as a function of the indices $2n$. The higher-order modes $(n > 14)$ have very small coefficients and do not play an important role in the reconstructed beam. A point to stress here is that, in order to optimize the functionality of the method, in the normalization of the transverse coordinates the width W should be smaller than the width of the square profile, otherwise the expansion requires a larger number of modes for describing the beam profile with accuracy. For the results presented here we have considered the value $d = 4$. In Fig. 2(b) we also plot the error in the approximation, as defined in Eq. (14). The error is $\sim 3\%$ for $N = 10$ and falls under 1% for $N > 30$, which means that the reconstruction of the beam can be very accurate using only a few modes.

For another example, we consider a one-dimensional half-sine profile centered around the axis ($\xi = 0$)

$$E(\xi)|_{\tau=0} = E_0\sin(\xi+d)\left[h(\xi+d) - h(\xi-d)\right], \quad (16)$$

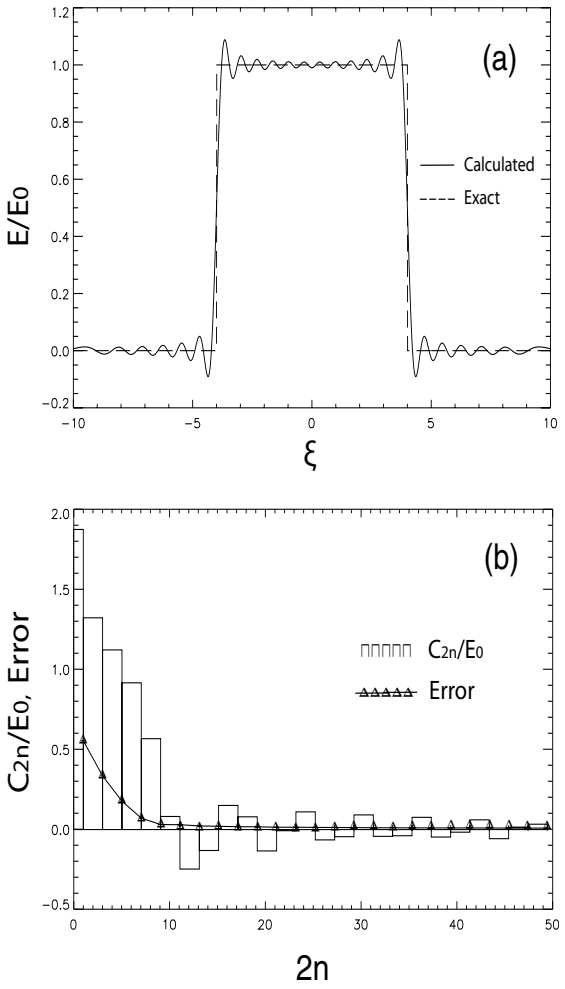

FIG. 2: (a) Profile of a one-dimensional square beam, as reconstructed using $N = 50$ modes. (b) Coefficients of the even Gaussian-Hermite modes, corresponding to the previous expansion, and expansion error as a function of the even indices.

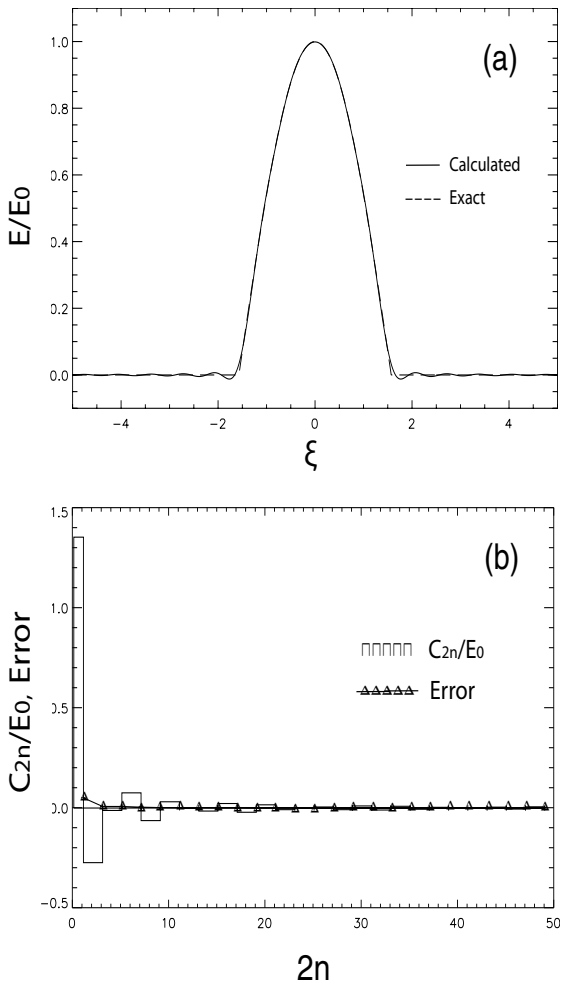

FIG. 3: (a) Profile of a one-dimensional half-sine beam, reconstructed using $N = 50$ modes. (b) Coefficients of the even modes and expansion error as a function of the even indices.

where again the coefficients are non-zero only for even indices. In Fig. 3(a) we show the reconstructed profile of the half-sine beam, where $d = \pi/2$ and $N = 50$ modes were used. The approximation is very accurate across all the beam. In Fig. 3(b), the coefficients of the even modes are plotted as a function of the indices $2n$. It is seen that only the modes $n < 8$ play an important role in the reconstructed beam. From Fig. 2(b), where the expansion error is plotted, ones comes to the same conclusion. The error in the approximation is $\sim 7\%$ for $N = 2$ and falls under 1% even from $N = 4$.

For the solution of the beam tracing equations and the transport equation, the formalism of Ref. 10 is followed. The beam tracing equations are the same for all the higher-order modes, because all the quantities are calculated on the reference ray. The general form of the amplitude transport equation reads

$$\frac{d\bar{C}_{mn}}{d\tau} + (\bar{\boldsymbol{e}}^* \cdot M[\bar{\boldsymbol{e}}] + \gamma)\bar{C}_{mn} = 0, \qquad (17)$$

where $M[\bar{\boldsymbol{e}}] = -\nabla \times (\nabla s \times \bar{\boldsymbol{e}}) - \nabla s \times (\nabla \times \bar{\boldsymbol{e}})$. Combination of Eq. (17) for $\bar{C}_{mn} = |\bar{C}_{mn}|e^{i\arg(\bar{C}_{mn})}$ with its conjugate equation yields Eq. (10) for $|\bar{C}_{mn}|^2$, as well as an equation for $\arg(\bar{C}_{mn})$

$$\frac{d[\arg(\bar{C}_{mn})]}{d\tau} = \frac{i}{2}(\bar{\boldsymbol{e}}^* \cdot \hat{M}[\bar{\boldsymbol{e}}] - \bar{\boldsymbol{e}} \cdot \hat{M}[\bar{\boldsymbol{e}}^*]), \qquad (18)$$

which is the same for all modes, as the second part consists of variables relevant to the reference ray. Eq. (17), on the other hand, is in general not the same for all modes, because the absorption coefficient γ depends on the wave-vector, which is different for each mode. In specific, the wave-vector corresponding to the propagation of the mode (m, n) is

$$\boldsymbol{k_{mn}} = \nabla(\kappa s - \Theta_{mn}) = \boldsymbol{k} - \frac{d\Theta_{mn}}{d\tau}\nabla\tau, \qquad (19)$$

where $\boldsymbol{k} = \kappa\nabla s$ is the wave-number corresponding to the reference ray, a solution of the ray-tracing equations, and

$\nabla\tau$ may be calculated from the components of the ray-tracing equation involving $d\boldsymbol{r}/d\tau$. The absorption coefficient can be evaluated directly from analytical models (e.g. Ref. 12) or by solving the hot plasma dispersion relation as e.g. done in Ref. 14 (numerical results are displayed in Sec. V).

In order to complete the solution, what remains to be calculated is the phase shift Θ_{mn}. Its importance is further elucidated in the next section. In terms of Ref. 10, Θ_{mn} is given by

$$\Theta_{mn} = (m+n+1)\int_0^\tau \mathcal{N} d\tau, \tag{20}$$

where $\mathcal{N}$ is an arbitrary function along the reference ray, which however should satisfy the relation

$$\frac{\partial^2 H}{\partial k_\alpha \partial k_\beta}\frac{\partial \xi_i}{\partial x_\alpha}\frac{\partial \xi_j}{\partial x_\beta} = \kappa \mathcal{N}\delta_{ij}. \tag{21}$$

This relation is actually a different form of Eq. (40) of Ref. 10, and must be satisfied because it is the solvability condition of Eq. (24c) in Ref. 10, one of the equations of half-order that arises after (7) is inserted in the wave equation and combined with Eq. (5) of Ref. 10, i.e.

$$\frac{1}{2}\delta_{ij}\frac{\partial^2 \Phi_{mn}}{\partial \xi_i \partial \xi_j} + \left(m+n+1-\frac{1}{2}\delta_{ij}\xi_i\xi_j\right)\Phi_{mn} = 0. \tag{22}$$

The latter equation is a property of the two-dimensional Gaussian-Hermite functions, derived by a summation of the respective one-dimensional equations

$$\frac{d^2\phi_n}{\partial \xi^2} + (2n+1-\xi^2)\phi_n = 0. \tag{23}$$

This formalism has met successful application to the case of a Gaussian beam. However, for applying to the case of an arbitrary beam, a reconsideration is needed. More specifically, the condition imposed above is too restrictive for the form of the beam. Only beams with physical behaviour obeying the specific symmetry prescribed by Eq. (21), i.e. $\partial^2_{\alpha\beta}H\partial_\alpha\xi_1\partial_\beta\xi_1 = \partial^2_{\alpha\beta}H\partial_\alpha\xi_2\partial_\beta\xi_2$ (∂_α is the partial derivative with respect to x_α and $\partial_{\alpha\beta}$ is the partial derivative with respect to k_α, k_β) can be modelled. A generalization can be made by defining two quantities μ, ν, one per transverse direction, as multipliers of Eqs. (23) [26]. The introduction of such quantities is reflected in Eq. (22) in the following manner

$$\frac{1}{2}\mu\frac{\partial^2\Phi_{mn}}{\partial\xi_1^2} + \frac{1}{2}\nu\frac{\partial^2\Phi_{mn}}{\partial\xi_2^2} + \left(m\mu + n\nu + \frac{\mu+\nu}{2} - \frac{1}{2}\mu\xi_1^2 - \frac{1}{2}\nu\xi_2^2\right)\Phi_{mn} = 0.$$

In the sequence described above, this results into the following relations

$$\frac{\partial^2 H}{\partial k_\alpha \partial k_\beta}\frac{\partial \xi_i}{\partial x_\alpha}\frac{\partial \xi_i}{\partial x_\beta} = \kappa\mathcal{N}(\mu\delta_{i,1} + \nu\delta_{i,2}), \tag{24}$$

actually splitting the relation (21) into two separate relations, which do not impose any restriction on the physics of the beam and can be applied in general cases. One can show that the generalization does not affect the form of the beam tracing equations as given in (9) [26]. In this framework, the relation for the phase shift is modified to

$$\Theta_{mn} = \left(m+\frac{1}{2}\right)\int_0^\tau \mu\mathcal{N}d\tau + \left(n+\frac{1}{2}\right)\int_0^\tau \nu\mathcal{N}d\tau. \tag{25}$$

Eqs. (24) relate the quantities μ, ν, $\mathcal{N}$ to the Hamiltonian and the transformation between the beam and the laboratory coordinates. In applications, these can serve for determining the terms $\mu\mathcal{N}$ and $\nu\mathcal{N}$ appearing in the phase-shift [see Eq. (25)]. For example, in the case of propagation in vacuum along the $x-$axis of the lab coordinate system, where the Hamiltonian is $H = c^2k^2/(2\omega^2) - 1/2$ and the relation between the beam and lab coordinates is $\xi_q = q/W_q$ ($q = y, z$), the result is $\mu\mathcal{N} = c^2/(\omega^2 W_y^2)$ and $\nu\mathcal{N} = c^2/(\omega^2 W_z^2)$. In the above, issues related to the deal of arbitrariness of μ, ν, $\mathcal{N}$ have not been discussed. A thorough investigation of the relation between μ, ν, $\mathcal{N}$ and the choice of beam coordinates is presented in Ref. 26.

IV. PARAMETERIZATION OF NON-GAUSSIAN BEAMS

In most applications relevant to fusion involving wave beams, the beams are considered to be of Gaussian shape. As pointed out in the Introduction, for most cases this is a justified, or at least desirable, situation. A Gaussian beam can be described by a set of few parameters, the most important of which are the beam width, which measures the transversal extent of the beam, and the curvature radius, which reflects the focusing of the beam. The beam width is usually defined as the distance from the maximum where a decrease of a factor of $1/e$ in the amplitude occurs ($1/e$-width), but also the definition as the full width at half the maximum (FWHM) is occasionally met. The curvature radius is the radius of the spherical curve defined by the shape of the wave-front.

In the case of non-Gaussian beams, the standard definitions of the parameters usually fail in properly describing the beam. For example, the $1/e$ definition may estimate wrongly the spot size of the beam, because the field usually falls below $1/e$ at more than one locations along the transversal plane. Also, in some cases the spherical approximation for the wave-front may be inadequate or even irrelevant. In such cases, it is necessary to revise the parameterization for the beam. The whole outlook of parameterization is important, because it provides a simple, yet effective, description of the global aspects of the beam using few parameters. The transversal extent and the structure of the wave-front completely characterize the main beam behaviour without referring to the local variations in the wave field distribution, which are

time-consuming to calculate and in many practical applications are even not of interest.

The characterization of arbitrary beams can be made by generalizing the parameters already defined for the Gaussian beam. Based on the knowledge of the amplitude map in the transverse plane, the generalized parameters may be defined in terms of the moments of the amplitude distribution of the electric field

$$\langle x^m y^n \rangle = \frac{\int_{-\infty}^{\infty} x^m y^n |\bar{E}(x,y)|^2 dxdy}{\int_{-\infty}^{\infty} |\bar{E}(x,y)|^2 dxdy}. \qquad (26)$$

In this paper, we will deal with the generalization of the most important parameter, the beam width. In terms of the theory of lasers and modern optics [18, 27], the width of arbitrary beams is accurately described by a two dimensional symmetric matrix

$$\hat{w}^2 = 2 \begin{bmatrix} \langle x^2 \rangle - \langle x \rangle^2 & \langle xy \rangle - \langle x \rangle \langle y \rangle \\ \langle xy \rangle - \langle x \rangle \langle y \rangle & \langle y^2 \rangle - \langle y \rangle^2 \end{bmatrix}. \qquad (27)$$

In this matrix, the subtracted terms describe any decentering of the beam, whereas the non-diagonal terms relate to any coupling of the transverse directions in the field amplitude. We should note that a coordinate system can be found where the coupling of the transverse direction vanishes. Such an aligned coordinate system is preferable, because then $\hat{w}$ becomes diagonal

$$\hat{w}^2 = \begin{bmatrix} w_y^2 & 0 \\ 0 & w_z^2 \end{bmatrix}, \qquad (28)$$

with $w_q = \sqrt{2(\langle q^2 \rangle - \langle q \rangle^2)}$ the generalized width per direction $q = x, y$. For a Gaussian beam, the generalized width is easily found to coincide with the definition of the $1/e$ width for the beam.

We apply the above to the case of a non-Gaussian beam expressed as a superposition of Gaussian-Hermite modes treated above. The non-Gaussian field is suitably written as the superposition of the lowest-order Gaussian mode (main mode) and a sum of higher-order terms with the same polarization acting as correction/deformation terms to the main mode: $\bar{E} = \bar{E}_{00} + \sum_{m,n} \bar{E}_{mn}$. Implementing the beam tracing form for the particular solution $\bar{E}_{mn}$, we obtain for the square $|\bar{E}|^2 = \bar{E}\bar{E}^*$ of the electric field

$$|\bar{E}|^2 = \frac{|\bar{C}_{00}|^2}{\pi} e^{-\xi_1^2} e^{-\xi_2^2} [H_0^2(\xi_1) H_0^2(\xi_2) + \sum_{mnkl} \frac{|\bar{r}_{mn}||\bar{r}_{kl}| \cos(\theta_{mn} - \theta_{kl})}{\sqrt{2^{m+n+k+l} m!n!k!l!}} H_{mk}(\xi_1) H_{nl}(\xi_2) + 2 \sum_{mn} \frac{|\bar{r}_{mn}| \cos\theta_{mn}}{\sqrt{2^{m+n} m!n!}} H_{0m}(\xi_1) H_{0n}(\xi_2)], \qquad (29)$$

where $\bar{C}_{00}$ is the amplitude of the main mode, $\bar{r}_{mn} = \bar{C}_{mn}/\bar{C}_{00}$ is the ratio of the amplitude of the mode (m,n) over the main mode, $\theta_{mn} = \Theta_{mn} - \Theta_{00} - \arg(\bar{r}_{mn})$ is the total phase-shift of the mode (m,n) and the representation $H_{mn}(x) = H_m(x) H_n(x)$ is introduced for the sake of simplicity. In the sums, the relation $\bar{z} + \bar{z}^* = 2Re(z)$ for complex numbers has been used. A more clear representation of (29) is possible, if the sum on m, n, k, l is separated into the sum of terms with $(m,n) = (k,l)$ and the sum of the remaining terms. The simplification owes to the fact that the sum of terms with equal pairs of indices contains only quadratic terms, while the other sum contains the coupling terms. Using also Kronecker delta symbols as $\delta'_{mknl} = 1 - \delta_{mk}\delta_{nl}$, the field becomes

$$|\bar{E}|^2 = \frac{|\bar{C}_{00}|^2}{\pi} e^{-\xi_1^2} e^{-\xi_2^2} [H_0^2(\xi_1) H_0^2(\xi_2) + \sum_{mn} \frac{|\bar{r}_{mn}|^2}{2^{m+n} m!n!} H_m^2(\xi_1) H_n^2(\xi_2) + \sum_{mnkl} \frac{|\bar{r}_{mn}||\bar{r}_{kl}| \cos(\theta_{mn} - \theta_{kl})}{\sqrt{2^{m+n+k+l} m!n!k!l!}} H_{mk}(\xi_1) H_{nl}(\xi_2) \delta'_{mknl} + 2 \sum_{mn} \frac{|\bar{r}_{mn}| \cos\theta_{mn}}{\sqrt{2^{m+n} m!n!}} H_{0m}(\xi_1) H_{0n}(\xi_2)]. \qquad (30)$$

Based on the electric field of Eq. (30), the generalized width matrix can be derived. In the frame (ξ_1, ξ_2), the matrix is diagonal and normalized, so Eq. (28) can be used. The matrix form in the lab frame depends on the transformation from the beam coordinates (τ, ξ_1, ξ_2) to the lab coordinates (x, y, z), which is directly known from the solution of the beam tracing equations for the tensor $\phi_{\alpha\beta}$. In the calculations, the properties of the orthogonality of the Hermite polynomials are taken into account. The first-order moment for the coordinate ξ_1 is

$$\langle \xi_1 \rangle = \left(1 + \sum_{mn} |\bar{r}_{mn}|^2\right)^{-1} \left[\sum_{mnkl} |\bar{r}_{mn}||\bar{r}_{kl}| \delta_{nl} \cdot \cos(\theta_{mn} - \theta_{kl}) \left(\sqrt{\frac{m}{2}} \delta_{m,k+1} + \sqrt{\frac{k}{2}} \delta_{m,k-1} \right) + 2 \sum_{mn} |\bar{r}_{mn}| \cos\theta_{mn} \sqrt{\frac{m}{2}} \delta_{m,1} \delta_{n,0} \right], \qquad (31)$$

and the result for ξ_2 can be obtained by interchanging m with n and k with l. The second order moment for ξ_1, and accordingly for ξ_2 by interchange, is

$$\langle \xi_1^2 \rangle = 1 + \left(1 + \sum_{mn} |\bar{r}_{mn}|^2\right)^{-1} \left[\sum_{mnkl} |\bar{r}_{mn}||\bar{r}_{kl}| \delta_{nl} \cdot \cos(\theta_{mn} - \theta_{kl}) [\sqrt{m(m-1)} \delta_{m,k+2} + \sqrt{k(k-1)} \delta_{m,k-2}] + 2 \sum_{mn} |\bar{r}_{mn}| \cos\theta_{mn} \sqrt{m(m-1)} \delta_{m,2} \delta_{n,0} \right], \qquad (32)$$

and one may calculate the width matrix using (28).

Let us illustrate the analytic calculations with the study of the simplest case of only one additional higher-

order mode (m,n). The square field in this case is just

$$|\bar{E}|^2 = \frac{|\bar{C}_{00}|^2}{\pi} e^{-\xi_1^2} e^{-\xi_2^2} [H_0^2(\xi_1) H_0^2(\xi_2) + \frac{|\bar{r}_{mn}|^2}{2^{m+n} m! n!} H_m^2(\xi_1) H_n^2(\xi_2) + \frac{2|\bar{r}_{mn}|}{\sqrt{2^{m+n} m! n!}} H_{0m}(\xi_1) H_{0n}(\xi_2) \cos\theta_{mn}], \quad (33)$$

while the moments of ξ_1 are

$$\langle \xi_1 \rangle = \frac{|\bar{r}_{mn}|}{1+|\bar{r}_{mn}|^2} \cos\theta_{mn} \sqrt{2m} \delta_{m,1} \delta_{n,0}, \quad (34a)$$

$$\langle \xi_1^2 \rangle = \frac{1}{2} + m \frac{|\bar{r}_{mn}|^2}{1+|\bar{r}_{mn}|^2} + \frac{|\bar{r}_{mn}|}{1+|\bar{r}_{mn}|^2} \cos\theta_{mn} \sqrt{m(m-1)} \delta_{m,2} \delta_{n,0}. \quad (34b)$$

The generalized width in the ξ_1-direction, according to Eq. (28), reads

$$w_1^2 = 1 + 2m \frac{|\bar{r}_{mn}|^2}{1+|\bar{r}_{mn}|^2} + \frac{2|\bar{r}_{mn}|}{1+|\bar{r}_{mn}|^2} \cos\theta_{mn} \delta_{n,0} \cdot \left[\sqrt{m(m-1)} \delta_{m,2} - m \frac{2|\bar{r}_{mn}|}{1+|\bar{r}_{mn}|^2} \cos\theta_{mn} \delta_{m,1} \right], \quad (35)$$

with all the results being interchangeable for the ξ_2-direction. We should note that in this framework, where we used normalized transverse coordinates ξ_1, ξ_2, the generalized widths are also normalized to the same factors (normally the $1/e$-widths). For example, in the ξ_1-direction, the result (35) can be analyzed as follows: for $n \neq 0$ the width is equal to

$$w_1^2|_{n\neq 0} = 1 + 2m \frac{|\bar{r}_{m0}|^2}{1+|\bar{r}_{m0}|^2},$$

whereas when $n = 0$, if $m = 1$ we have

$$w_1^2|_{m=1,n=0} = 1 + 2\frac{|\bar{r}_{10}|^2}{1+|\bar{r}_{10}|^2} - \left(\frac{2|\bar{r}_{10}|}{1+|\bar{r}_{10}|^2} \right)^2 \cos^2\theta_{10},$$

while if $m = 2$ the result is

$$w_1^2|_{m=2,n=0} = 1 + 4\frac{|\bar{r}_{20}|^2}{1+|\bar{r}_{20}|^2} + \sqrt{2}\frac{2|\bar{r}_{20}|}{1+|\bar{r}_{20}|^2} \cos\theta_{20}.$$

Notice that the only cases where the phase-shift of the mode has an effect on the generalized width are $(m,n) = (1,0),(2,0),(0,1),(0,2)$. In all the other cases, the generalized width is always larger that the characteristic width of the main mode, increases with the mode numbers and does not depend on the phase shift.

V. NON-GAUSSIAN EC PROPAGATION AND ABSORPTION IN A PLASMA SLAB

As an application, we study the perpendicular propagation and absorption of a non-Gaussian EC beam in a simplified plasma geometry (slab). The medium is confined in the region $-a \leq x \leq a$ along the $x-$axis, while it is unlimited in the other directions y, z of the laboratory frame. The static magnetic field is along the $z-$axis, and all the properties of the plasma are assumed to be functions only of the $x-$coordinate. The wave beam is launched from the low-field side at $x = x_0 = a$ in the negative $x-$direction ($k_{x0} < 0, k_{y0} = k_{z0} = 0$), and its electric field is the superposition of two real-valued Hermite-Gaussian modes with the same polarization, the lowest-order Gaussian $(0,0)$ and a higher-order mode (m,n). In the following, cold plasma propagation is assumed, i.e. hot plasma effects appear only in the amplitude and not in the polarization of the wave.

The analytical solution of the beam tracing equations for this problem has been obtained by Poli *et al.* [28]. The simplification for this case is that the dispersion function for quasi-perpendicular propagation reduces to a quadratic form $D = D_{ij} k_i k_j / 2 - 1/2 = 0$ $(i,j = x,y,z)$, with a dispersion tensor that is diagonal

$$\hat{D}^M(x) = \begin{bmatrix} D_{xx}^M(x) & 0 & 0 \\ 0 & D_{yy}^M(x) & \\ 0 & 0 & D_{zz}^M(x) \end{bmatrix}, \quad (36)$$

where $M = O, X$ refers to the polarization of the wave. For the different polarizations, the tensor elements are

$$D_{xx}^O = D_{yy}^O = \frac{c^2}{\omega^2} \frac{1}{\mathcal{P}}, \quad D_{zz}^O = \frac{c^2}{\omega^2},$$

$$D_{xx}^X = D_{yy}^X = \frac{c^2}{\omega^2} \frac{\mathcal{S}}{\mathcal{S}^2 - \mathcal{D}^2}, \quad D_{zz}^X = \frac{c^2}{\omega^2} \left(\frac{2\mathcal{S}}{\mathcal{S}^2 - \mathcal{D}^2} - 1 \right),$$

where $\mathcal{S}, \mathcal{D}, \mathcal{P}$ are the standard cold-plasma parameters (see Ref. 11). The dispersion function, which is the Hamiltonian for the reference ray, does not depend on the coordinates y, z, and thus the wave-vectors k_y, k_z are constantly zero throughout the propagation. Also, the wave-number k_x is fully determined by the dispersion relation, so the only ray-tracing equation of practical interest is the one involving $dx/d\tau$

$$k_x = -\frac{1}{\sqrt{D_{xx}^M}}, \quad \frac{dx}{d\tau} = \frac{\partial D}{\partial k_x} = \sqrt{D_{xx}^M}. \quad (37)$$

In this context, τ is a function only of x and the normalized transverse coordinates describing the amplitude profile are just y/W_y and z/W_z, where W_y, W_z are the principal widths in each perpendicular direction.

The solution of the beam tracing equations for the wave-front curvature and the beam width are [28]

$$\bar{s}_{jj}(x) = \frac{\bar{s}_{jj}(x_0)}{1 + \bar{s}_{jj}(x_0) l_j(x)}, \quad (38)$$

where l_j are the effective lengths defined by the relations

$$\frac{c}{\omega} l_j(x) = \int_0^\tau D_{jj}^M(\tau')d\tau' = -\int_{x_0}^x \frac{D_{jj}^M(x')}{\sqrt{D_{xx}(x')}}dx', \quad (39)$$

with the equation for the reference ray used for changing the integration variable from τ to x. The beam-tracing solution can be expressed in terms of the real and imaginary parts of $\bar{s}_{jj}$ and their initial values $\bar{s}_{jj}(x_0) = \bar{s}_{jj0}$. For the tensor ϕ_{jj}, which describes the beam width

$$\phi_{jj} = \frac{\phi_{jj0}}{(1 + s_{jj0} l_j)^2 + (\phi_{jj0} l_j)^2}. \quad (40)$$

The elements ϕ_{yy}, ϕ_{zz} are connected to the principal widths in each perpendicular direction

$$\kappa\phi_{yy} = \frac{1}{W_y^2}, \quad \kappa\phi_{zz} = \frac{1}{W_z^2}. \quad (41)$$

This connection can be established through the expression of the quadratic form ϕ in the beam and lab coordinates, which reads $2\phi = \xi_1^2 + \xi_2^2 = \kappa(\phi_{yy} y^2 + \phi_{zz} z^2)$. The solution for the principal width can be expressed in terms of the initial width and radius of curvature as follows

$$\frac{W_j^2}{W_{j0}^2} = \left(1 + \frac{l_j}{\kappa R_{j0}}\right)^2 + \frac{l_j^2}{\kappa^2 W_{j0}^2}. \quad (42)$$

The general form of Eq. (25) for Θ_{mn}, under the choice $\arg(\bar{r}_{mn}) = 0$, yields for the total phase shift

$$\theta_{mn}(x) = \frac{c^2}{\omega^2}\left(m\int_{x_0}^x \frac{D_{yy}^M}{W_y^2}dx' + n\int_{x_0}^x \frac{D_{zz}^M}{W_z^2}dx'\right). \quad (43)$$

The solution of the amplitude transport equation is

$$\frac{C_{mn}^2(x)}{C_{mn}^2(x_0)} = \sqrt{\frac{D_{xx}(x)}{D_{xx}(x_0)}}\frac{W_y(x_0)}{W_y(x)}\frac{W_y(x_0)}{W_z(x)} e^{-\int_{x_0}^x \gamma(x')dx'}, \quad (44)$$

where the absorption coefficient γ is evaluated based on the energy balance equation (see e.g. Ref. 12).

The evolution of the non-Gaussian beam is followed with the code NGBT, which applies the sequence presented in Sec. III. In particular, stress is given to the evolution of the generalized widths in comparison with the principal ones and in the evolution of the phase shift. In the simulations, the half-width of the plasma is $a = 100$ cm with the plasma density following a parabolic profile, $\omega_p^2(x)/\omega_c^2(0) = c_1 - c_2(x/a)^2$, with parameters $c_1 = 0.9$, $c_2 = 0.4$. If not zero, the plasma temperature follows a similar profile, $T_e(x) = T_1 - T_2(x/a)^2$ with $T_1 = 3$ KeV, $T_2 = 2.9$ KeV. The magnetic field varies according to a profile of the form $\omega_c(x)/\omega_c(0) = a/(a + \mathcal{A}x)$, where $\mathcal{A}$ is the aspect ratio, equal to 2.5 for the simulations. The wave frequency is $\omega/2\pi = 140$ GHz, either 1^{st} ($O-$mode) or 2^{nd} ($X-$mode) cyclotron harmonic depending on the value of the magnetic field. The mode E_{00} has a circularly symmetric initial amplitude profile with principal widths $W_{y0} = W_{z0} = 3.02$ cm, and a symmetric initial focusing with curvature radii $R_{y0} = R_{z0} = -82$ cm. We specify the initial amplitude of the higher-order mode in terms of the ratio of the power density corresponding to the mode over the total power density of the beam

$$\epsilon_{mn} = \frac{C_{mn}^2}{C_{00}^2 + C_{mn}^2} = \frac{r_{mn}^2}{1 + r_{mn}^2}. \quad (45)$$

Considering what was presented in the previous section, resulting in Eq. (35) and the ones following, one distinguishes the connection between the distribution of the beam energy among the modes and the beam geometry.

In Fig. 4 the generalized widths w_q ($q = y, z$) are shown, along with the widths of the main mode W_q (i.e. the principal widths), as a function of the coordinate x along the $O-$mode propagation for (a)(m, n)=$(2, 1)$ and (b) (m, n)=$(0, 2)$, where in both cases $\epsilon_{mn} = 0.1$. In Fig. 4(a), the generalized width is constantly larger from the principal one in both directions. In fact, the two widths in this case are almost proportional, because the generalized width does not depend of the phase shift [see Eq. (35)]. In the case of 4(b), the width in the $y-$direction coincides with the principal one because $m = 0$. In the other direction, the effect of the phase shift is obvious, and the variation of the beam width along the propagation path is significant. The width begins with an initial value much larger than the one of the main mode, however it converges to W_{z0} as the beam reaches its waist. The non-monotonic variation of the generalized width is owed to the dependence on θ_{mn}.

In Fig. 5 we present results for $X-$mode propagation, where the general behaviour is the same as in the previous case of the O-mode. In 5(a) the widths in the $z-$direction are compared for the case (m, n)=$(1, 3)$ and $\epsilon_{mn} = 0.05, 0.3$. It is obvious that the difference from the width of the main mode increases for larger values of the energy ratio. This was expected according to the formulas (35), which imply that the the width increases as a function of (m, n) and ϵ_{mn}. In Fig. 5(b) the widths in the $y-$direction are shown for (m, n)=$(1, 0)$ and $\epsilon_{mn} = 0.2, 0.5$. We can observe again the effect of the phase shift on the generalized width, which for this case, due to the small order of the additional mode, is not so intense and the generalized width attains values close to the principal width, even in the case $\epsilon_{mn} = 0.5$ where half the power of the beam is contained in the mode.

The evolution of the total phase shift of the mode (m, n) along the propagation is shown in Fig. 6(a), for both the $O-$ and $X-$mode with (m, n)=$(0, 2)$ and $\epsilon_{mn} = 0.1$. The variation of the phase shift in the plasma is significant in both cases and as a consequence the generalized width is not simply proportional to the Gaussian width and can become smaller than it. The phase-shift exhibits a different behaviour for the two cases, which is due to the dielectric tensor and the principal widths having different functional forms [cf. Eq. (43)]. In Fig. 6(b) the amplitudes of the different modes C_{00}, C_{mn} are compared, both for cold ($T_e = 0$) and hot plasma ($T_e \neq 0$

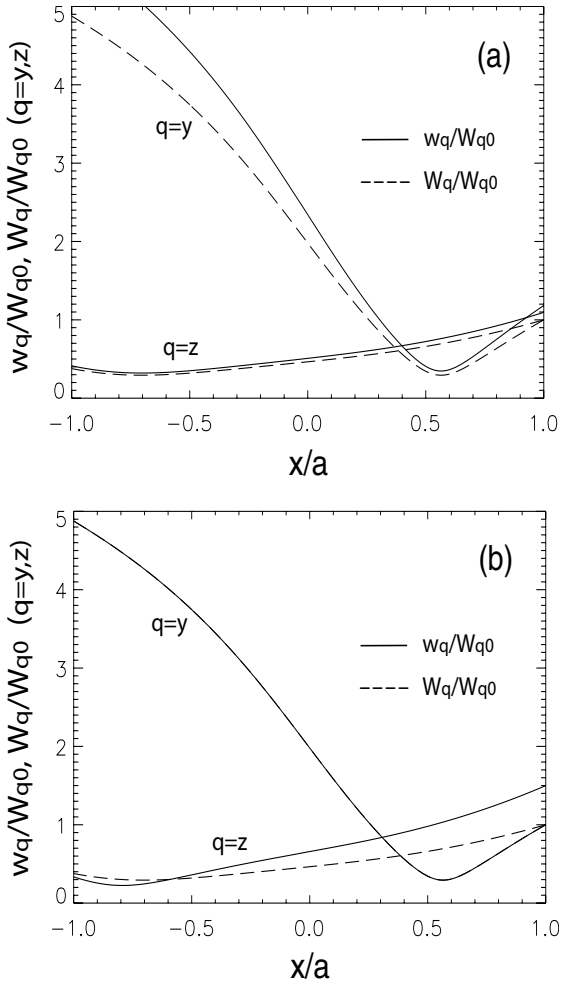

FIG. 4: Evolution of the generalized widths in the $y-, z-$direction for $O-$mode propagation with (a) (m,n)=$(2,1)$, (b) (m,n)=$(0,2)$ and $\epsilon_{mn} = 0.1$.

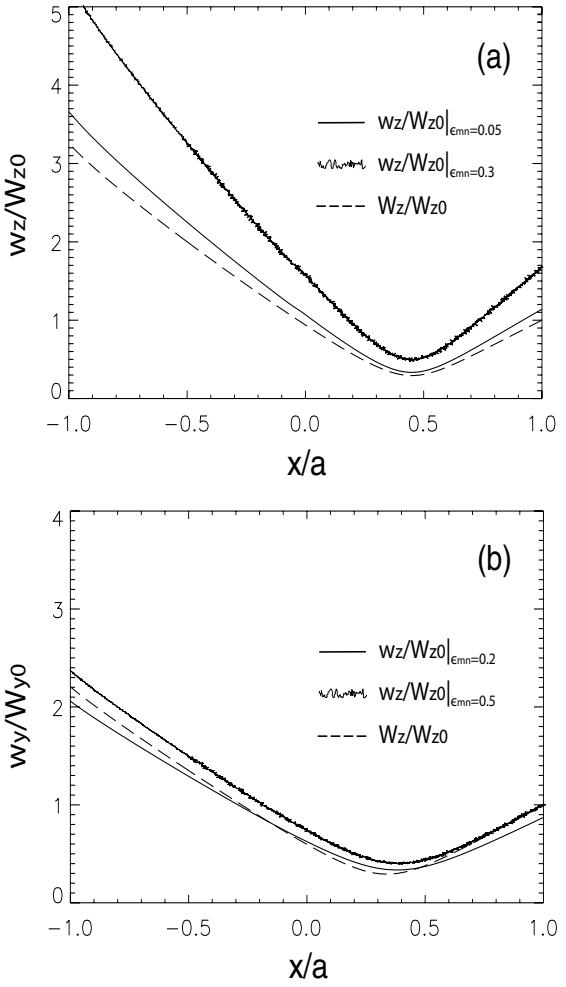

FIG. 5: Generalized widths for $X-$mode propagation (a) in the $z-$direction with (m,n)=$(1,3)$ and $\epsilon_{mn} = 0.05, 0.3$, (b) in the $y-$direction with (m,n)=$(1,0)$ and $\epsilon_{mn} = 0.2, 0.5$.

and according to the profile specified) $O-$mode propagation with (m,n)= $(2,1)$ and $\epsilon_{mn} = 0.1$. In the damping of the wave in the resonance layer, it is seen that the two modes are damped with approximately equal rates. The difference in the wave-vectors of the modes is small for suggesting different absorption rates of the different modes. As a result, the ratio r_{mn} for these cases does not vary significantly in the course of propagation, and thus the effect of the EC absorption on the width is very small. This effect however becomes important for higher-order modes. In Fig. 6(c) the ratio r_{mn} is shown for the cases $(m,n) = (1,1), (8,8)$, and in the second case the variation of r_{mn} within the resonance layer is significant.

The problem of wave propagation considered above is addressed in simplified plane geometry that allows a direct solution of the electric field without resorting to asymptotic techniques [29]. A wave beam of given frequency is modelled by a superposition of plane waves, each with a different value of the parallel wave vector k_z at the edge of the plasma (x = a). Because in this geometry the equilibrium is independent of z, y, both $k_z = k_{||}$ and k_y are conserved. The propagation of plane waves can be easily calculated, and the field at each point x can then be reconstructed through the superposition of the plane waves. One arrives at the following equation

$$\bar{\boldsymbol{E}}(x,z) = \int_{-\infty}^{\infty} \bar{\boldsymbol{\mathcal{E}}}(a,k_z) e^{-ik_z z - i\int_a^x k_x(k_z,x')dx'} \frac{dk_z}{2\pi}, \quad (46)$$

where $\bar{\boldsymbol{\mathcal{E}}}(a,k_z) = \int_{-\infty}^{\infty} \bar{\boldsymbol{E}}(a,z) e^{ik_z z} dz$ is the Fourier transform of the initial field, and a similar equation for $\bar{\boldsymbol{E}}(x,y)$. The results of this method can directly be compared with our analytic and numerical results. The numerical implementation is done by the code ECPROP. The initial beam profile at x = a can be specified in real or wave-vector space. At each propagation instant, $k_\perp$ is solved for each $k_{||}$ from the cold plasma dispersion equation and the electric field is obtained from an inverse Fourier transform. For the calculation of the generalized widths, a subroutine was added to ECPROP, which com-

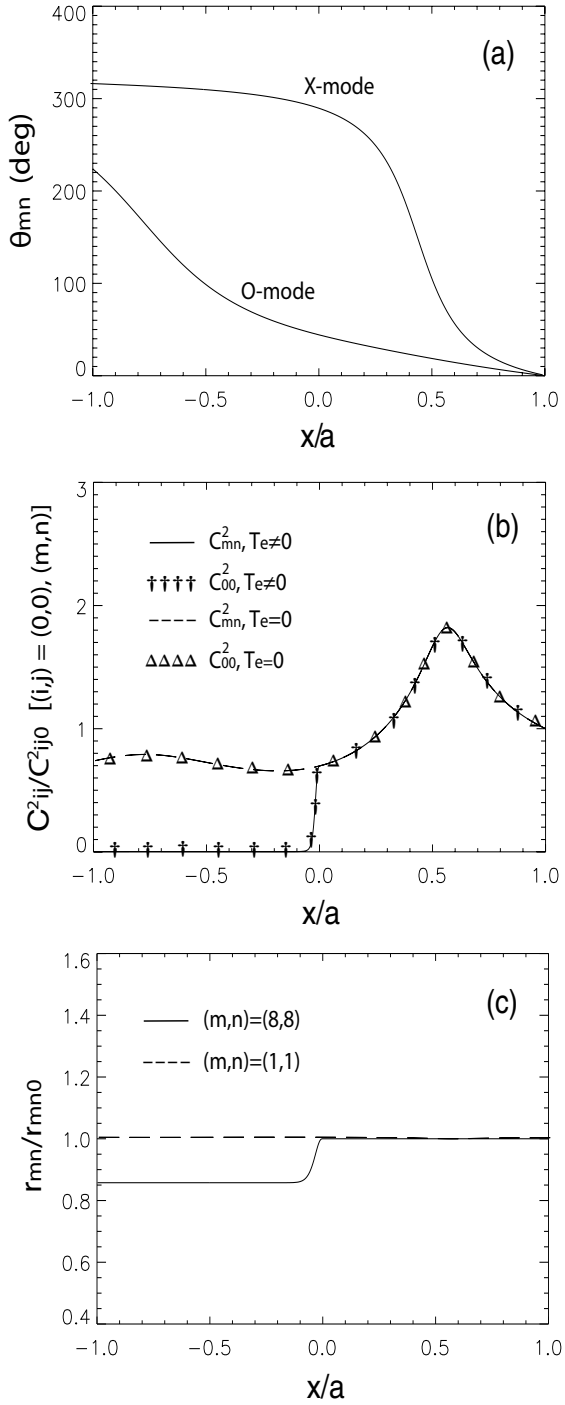

FIG. 6: (a) Total phase-shift θ_{mn} for $O-, X-$mode with (m,n)=(0, 2). (b) Amplitudes C^2_{00}, C^2_{mn} for cold ($T_e = 0$) and hot plasma ($T_e \neq 0$) $O-$mode with (m,n)=(2, 1). (c) Ratio r_{mn} for $X-$mode with (m,n)=(1, 1), (8, 8) ($\epsilon_{mn} = 0.1$).

putes the integrals involved [see Eqs. (26,28)]. In Fig. 7 the results of our code NGBT are compared to the results of ECPROP for the same wave and plasma parameters as in the numerical implementation of the previous subsection, but for cold plasma ($T_e = 0$). The parameters for the non-Gaussian mode are (m,n)=(0, 2) and $\epsilon_{mn} = 0.2$.

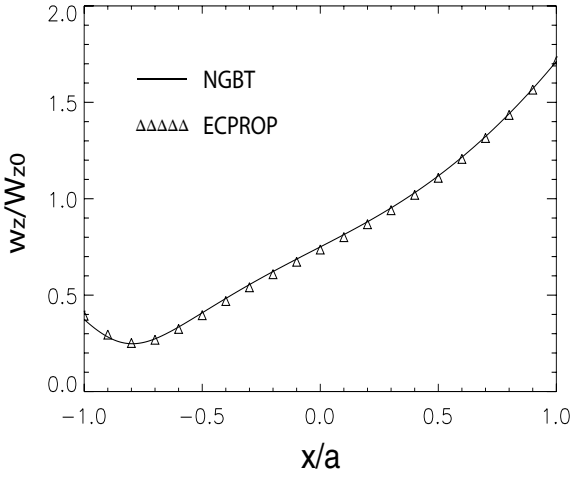

FIG. 7: Generalized width in the $z-$direction, as calculated by NGBT and ECPROP, for $O-$mode propagation with (m,n)=(0, 2) and $\epsilon_{mn} = 0.2$.

One can see that the agreement between the results of the two codes is very good.

VI. EFFICIENCY OF NON-GAUSSIAN BEAMS FOR ECRH TRANSMISSION

In this section, a possible application of non-Gaussian beams in ECRH transmission is discussed. There are cases where, despite their complexity, non-Gaussian beams obtain properties which make them preferable for particular applications. For example, reduction of the power density on the window between the transmission line and the vacuum vessel can be achieved by adding up higher-order Gaussian-Hermite modes to the zero-order (Gaussian) one in order to achieve a broader profile. In such a case, the properties of the beam are of particular interest and are shown to be advantageous.

Let us illustrate a specific example for the above. Using the electric field $E = E_{00} + E_{20} + E_{02}$, composed of three modes, an initially top-hat profile, broader than the one of a Gaussian beam, may be achieved. This is shown in Fig. 8(a), where the beam profile is plotted for the case $r_{20} = r_{02} = r/\sqrt{2}$ with $\epsilon = 0.1$. The square of the initial field in this case, emanating from Eq. (30), is just

$$E^2|_{x=0} = \frac{C^2_{00}}{\pi} e^{-\frac{y^2}{W_y^2} - \frac{z^2}{W_z^2}} H_0^2 \cdot \left\{ H_0^2 + \frac{r^2}{16}\left[H_2\left(\frac{y}{W_y}\right) + H_2\left(\frac{z}{W_z}\right)\right]^2 + \frac{r}{\sqrt{8}}\left[H_2\left(\frac{y}{W_y}\right) + H_2\left(\frac{z}{W_z}\right)\right]\right\}.$$

The propagation of the beam in the transmission line is actually propagation in vacuum. The solution of the beam tracing equations presented in the previous section describes the propagation, where one sets $D^M_{xx} = D^M_{yy} = D^M_{zz} = c^2/\omega^2$ for the dispersion tensor of vacuum and

$\omega_p = \omega_c = 0$, $T_e = 0$. Propagation starts at $x = 0$, where the profile is the one appearing in Fig. 8(a) and the beam has its waist ($1/R_0 \approx 0$) with a Gaussian width $W_0 = 1.98$ cm. In the transmission line, at the position $x = 1.51$ m there is a focusing mirror ($f = 90$ cm) in order to re-focus the beam before entering the plasma region. This results in a change in the value of the curvature radius, which can be calculated using the relation $1/f = 1/R_{mir} + 1/R'_0$ and (38) for calculating the curvature radius R_{mir} impinging on the mirror. After the mirror, the beam covers 32 cm before entering the plasma and approximately further 70 cm to reach the plasma center.

In Fig. 8(b) the generalized width in the $y-$direction is shown. The behaviour in the other transverse direction is similar due to the isotropy of vacuum. One can see that, for the biggest part of the propagation path, the non-Gaussian beam is more confined along the propagation and defocuses more slowly than a Gaussian beam. In other words, adding a higher-order mode to avoid too high heat loads at the window has the additional advantage of a better beam focusing inside the plasma. Here we should note that for the part of the propagation in the plasma the dispersion tensor of vacuum is retained (this is known as "vacuum calculation"). This does not affect the quality of the result presented in Fig. 8(b), as within this application our interest lies in the comparison of the Gaussian and non-Gaussian beam and not in the specific detail of the propagation.

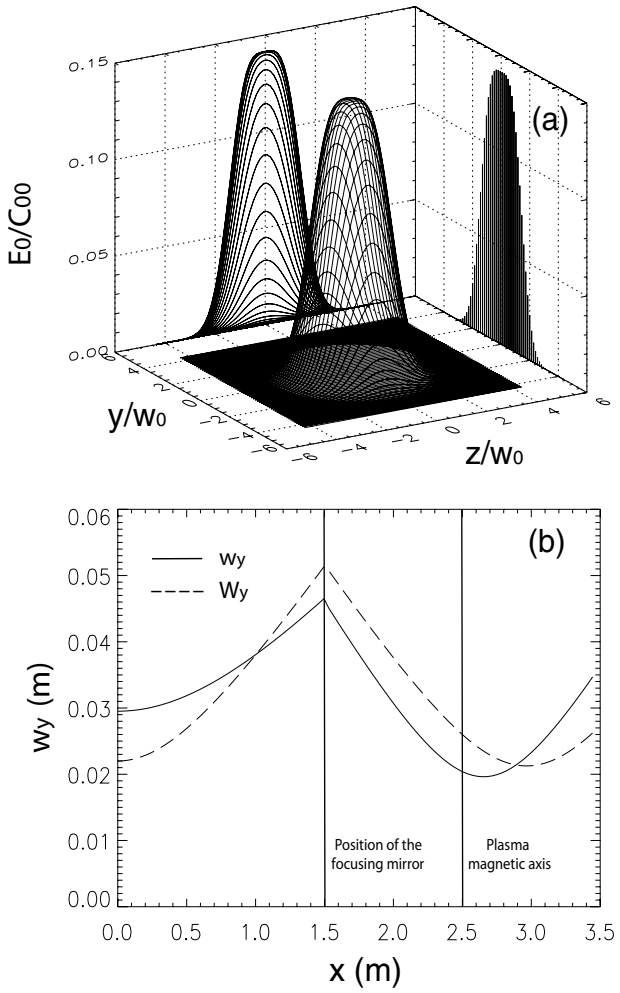

FIG. 8: (a) Electric field profile of the beam composed by $E = E_{00} + E_{20} + E_{02}$ for $\epsilon_{20} = \epsilon_{02} = 0.1/\sqrt{2}$. (b) Evolution of the generalized width in the $y-$direction for propagation in the transmission line and the plasma (vacuum calculation).

VII. SUMMARY - CONCLUSIONS

In this paper the propagation and absorption of non-Gaussian beams was formulated in terms of the pWKB beam-tracing asymptotic method. The need to study non-Gaussian beams emerges from the fact that, in ECRH/ECCD scenarios, the beams entering the plasma might not always be Gaussian or might be modified in the plasma e.g. due to localized absorption. It was discovered that the beam tracing formalism presented in Ref. 10 needed modifications in order to provide a proper description of arbitrary beam propagation in practical applications. The proper sequence for tracing arbitrary beams has been settled, and also generalized beam parameters have been introduced since the standard definitions, referring to the Gaussian beam, fail in properly describing non-Gaussian beams.

We applied the method to the propagation and absorption of the simplest non-Gaussian EC beam in a plasma slab. The generalized width increases as a function of (m, n) and ϵ_{mn}, and has a dependence on the total phase-shift of the mode only in the cases $(m, n) = (0, 1), (1, 0), (0, 2), (2, 0)$. The behaviour is similar both for $O-$ and $X-$mode propagation. The results were benchmarked in slab geometry against the code ECPROP, and a very good agreement was found in all cases. Also, an application of non-Gaussian beams in ECRH transmission was presented, where it was illustrated that by launching a proper multi-mode beam, a reduction of the power density on the window between the transmission line and the vacuum vessel can be achieved. Furthermore, a beam of this type was shown to defocus more slowly and to remain more localized than a Gaussian beam during the propagation in vacuum.

The work presented here opens the way for the modification of pWKB beam-tracing codes likes TORBEAM to include the propagation and absorption of arbitrary EC beams, as well as for the construction of a theory for the description of modifications in the beam profile during the propagation in the plasma.

Acknowledgments

The authors would like to thank Dr. E. Westerhof for the provision of the code ECPROP and Drs. F. Leuterer and D. Wagner for many useful discussions and for sup-

plying the data employed in Sec. VI. This work has been sponsored by the European Fusion Programme (Association EURATOM-Hellenic Republic) and the General Secretariat of Research and Technology. The sponsors do not bear any responsibility for the content of this work.

[1] V. Erckmann and U. Gasparino, Plasma Phys. Control. Fusion **36**, 1869 (1994).
[2] B. Lloyd, Plasma Phys. Control. Fusion **40**, A119 (1998).
[3] R. Prater, Phys. Plasmas **11**, 2349 (2004).
[4] I. B. Bernstein, Phys. Fluids **18**, 320 (1975).
[5] L. Friedland and I. B. Bernstein, Phys. Rev. A **22**, 1680 (1980).
[6] E. Mazzucato, Phys. Fluids B **1**, 1855 (1989).
[7] G. V. Permitin and A. Smirnov, Sov. Phys. JETP **82**, 395 (1996).
[8] Y. Kravtsov, G. W. Forbes, and A. A. Asatryan, Progress in Optics **XXIX**, 1 (1999).
[9] G. V. Pereverzev, Rev. Plasma Phys. **19**, 1 (1996).
[10] G. V. Pereverzev, Phys. Plasmas **5**, 3529 (1998).
[11] T. H. Stix, *Waves in Plasmas* (McGraw-Hill, New York, 1992).
[12] M. Bornatici, Nucl. Fusion **23**, 1153 (1983).
[13] D. G. Swanson, *Plasma Waves* (Academic, New York, 1989).
[14] E. Westerhof, Tech. Rep. 89-183, FOM-Rijnhuizen (1989).
[15] S. Nowak and A. Orefice, Phys. Fluids B **5**, 1945 (1993).
[16] E. Poli, A. G. Peeters, and G. V. Pereverzev, Comp. Phys. Commun. **136**, 90 (2001).
[17] D. Farina, Tech. Rep. FP 05/1, IFP-CNR (2005).
[18] A. E. Siegman, *Lasers* (Oxford University Press, 1986).
[19] L. D. Landau and E. M. Lifshitz, *The Classical Theory of Fields* (Pergamon Press, Oxford, 1997).
[20] S. Weinberg, Phys. Rev. **126**, 1889 (1962).
[21] Y. A. Kravtsov and Y. I. Orlov, *Geometrical Optics of Inhomogeneous Media* (Springer Verlag, Berlin, 1990).
[22] S. Choudary and L. B. Felsen, IEEE Trans. Antennas Prop. **AP-21**, 827 (1973).
[23] A. Bravo-Ortega and A. H. Glasser, Phys. Fluids B **3**, 529 (1991).
[24] O. Maj, Ph.D. thesis, University of Milan (2003).
[25] E. Poli, G. V. Pereverzev, A. G. Peeters, and M. Bornatici, Fusion Eng. Design **53**, 9 (2001).
[26] G. V. Pereverzev, to be submitted (2006).
[27] R. H. Dreggers, ed., *Encyclopedia of Optical Engineering* (Marcel-Dekker, 2003).
[28] E. Poli, G. V. Pereverzev, and A. G. Peeters, Phys. Plasmas **6**, 5 (1999).
[29] E. Westerhof, Plasma Phys. Control. Fusion **39**, 1015 (1997).